Ocean Engineering 253 (2022) 111315

Contents lists available at ScienceDirect

Ocean Engineering

journal homepage: www.elsevier.com/locate/oceaneng

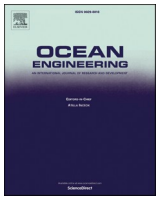

Characterization of spatio-temporal distributions of wave-induced pore pressure in a non-cohesive seabed: Amplitude-attenuation and phase-lag

Chang-Fei Li [a,b], Fu-Ping Gao [a,b,*]

[a] Institute of Mechanics, Chinese Academy of Sciences, Beijing, 100190, China
[b] School of Engineering Science, University of Chinese Academy of Sciences, Beijing, 100049, China

ARTICLE INFO

Keywords:
Flume observations
Analytical solution
Wave-induced pore pressure
Amplitude attenuation
Phase lag

ABSTRACT

While ocean waves propagating over a porous seabed, the amplitude of excess pore pressure would attenuate into the seabed (termed as "amplitude-attenuation"), which is always accompanied by "phase-lag". In this study, the amplitude-attenuation and the phase-lag phenomena in a fine-sand bed and a medium-sand bed were physically modeled in a large wave flume. A relative rigidity of soil-skeleton to pore-fluid is introduced to evaluate the seabed compressibility. Explicit expressions of the amplitude-attenuation and the phase-lag are derived and then validated with the experimental results. Parametric analyses indicate that, for the relative rigidity of the seabed much larger than 1.0, the amplitude-attenuation and the phase-lag along the non-dimensional soil depth would become more significant for larger wave period, but for smaller values of the combined rigidity-permeability parameter of the soil. A non-dimensional parameter (I_c) is further derived to characterize the combined effects of wave parameters and soil properties. Simplified spatio-temporal correlation of transient pore pressure is finally established for $I_c \gg 1.0$, indicating the more rapidly the pore pressure amplitude attenuates within the seabed, the more significant the phase-lag becomes, correspondingly.

1. Introduction

Wave-induced pore pressure in a porous seabed may lead to a reduction of effective stress and even the seabed liquefaction (see Jeng et al., 2007). The failures or instabilities of subsea structures under the action of wave loading have been frequently reported and intensively investigated, e.g., the instability of breakwaters (Smith and Gordon, 1983; Miyamoto et al., 1989; Groot et al., 2006; Jeng, 2018), the sinking or floatation of submarine pipelines (Christian et al., 1974; Sumer et al., 1999; Sumer, 2014; Qi et al., 2020), and the residual liquefaction or local scour around pile foundations (Sumer and Fredsøe, 2002; Li et al., 2011; Qi and Gao, 2014a,b). As well known, while ocean waves propagating over a porous seabed, the amplitude of excess pore pressure would attenuate into the seabed (termed as "amplitude-attenuation"), which is always accompanied by "phase-lag". Such amplitude-attenuation and phase-lag are the two key features for the spatio-temporal distributions of wave-induced pore pressures, which should be well predicted for underpinning the evolution of offshore foundations.

In the past few decades, wave-induced transient pore pressure phenomena have been intensively observed via flume modeling (e.g., Yamamoto et al., 1978; Maeno and Hasegawa, 1985; Zen and Yamazaki, 1990; Qi et al., 2019) and offshore field measurements (e.g., Mory et al., 2007; Michallet et al., 2009). Meanwhile, a few theoretical models were established based on various assumptions for the soil-skeleton and the pore-fluid of a porous seabed. The existing theoretical models can thereby be divided into three categories on the basis of different seabed assumptions (see Table 1): (1) a RS-IF seabed: rigid soil-skeleton with incompressible pore-fluid (Putnam, 1949; Reid and Kajirua, 1957), (2) a RS-CF seabed: rigid soil-skeleton with compressible pore-fluid (Moshagen and Tørum, 1975), and (3) an ES-CF seabed: elastic soil-skeleton with compressible pore-fluid (Yamamoto et al., 1978; Madsen, 1978). As listed in Table 1, the governing equations are different under various assumptions for the soil-skeleton and the pore-fluid of a porous seabed. For a RS-IF seabed, the governing equation is Laplace equation; for a RS-CF seabed, it is the diffusion equation; and for an ES-CF seabed, it is Biot's consolidation equation. Theoretical analyses indicated that, for a RS-IF seabed with an infinite thickness, the pore pressure amplitude would attenuate exponentially with the soil depth (Reid and Kajirua, 1957); but for a RS-CF seabed, the amplitude-attenuation would get more significant than that under the RS-IF assumption (Moshagen and Tørum, 1975). Compared with the "RS-IF" or the "RS-CF" seabed models, the ES-CF seabed models (e.g., the analytical solution by

* Corresponding author. Institute of Mechanics, Chinese Academy of Sciences, Beijing, 100190, China.
E-mail address: fpgao@imech.ac.cn (F.-P. Gao).

https://doi.org/10.1016/j.oceaneng.2022.111315
Received 29 June 2021; Received in revised form 27 February 2022; Accepted 9 April 2022
Available online 21 April 2022

Notation

A	Coefficient in Eq. (A4)
c	Coefficient in Eq. (2)
d	Water depth
d_{10}	Effective size of sand grains
d_{50}	Mean size of sand grains
d_s	Depth of the soil box in the flume
D_r	Relative density of sands
e	Void ratio under the in-situ condition
e_{max}	Maximum void ratio of the sand
e_{min}	Minimum void ratio of the sand
G	Gravitational acceleration
G	Shear modulus of the soil
G_s	Specific weight of the soil
H	Wave height
i	Imaginary number
I_c	Dimensionless parameter in Eq. (16)
K	Apparent bulk modulus of the porous seabed
k_s	Coefficient of permeability
k_{sat}	Permeability of the saturated soil
K_w	True bulk modulus of the pure water
K'	Apparent bulk modulus of the pore-fluid
L	Wave length
m	Coefficient in Eq. (2)
M	Longitudinal bulk modulus (or P-wave modulus)
n	Soil porosity
p	Wave-induced pore pressure within the soil
p_0	Amplitude of wave-induced pressure at the seabed surface
P_0	Absolute hydrostatic pore water pressure
P_b	Wave-induced pressure at the seabed surface
R_k	Stiffness ratio
S	Specific surface
S_0	Degree of saturation corresponding to a certain water content
S_r	Degree of saturation
T	Wave period
t	Time
z	Soil depth calculated from the mudline
z_a	Arbitrary soil depth in Fig. 1
η	Wave surface elevation
α	Coefficient in Eq. (1)
β	Coefficient in Eq. (2)
γ'	Buoyant unit weight of soil
γ_w	Unit weight of water
λ	Wave number
λ'	Coefficient in Eq. (1)
ν	Poisson's ratio
ΔT	Time-lag between the waves and the corresponding excess pore pressure
θ	Phase of the progressive waves
$\Delta\theta$	Phase-lag of the wave-induced pore pressure
ξ_1	Coefficient in Eq. (8)
ξ_2	Coefficient in Eq. (8)
ω	Angular frequency of the wave
ω'	Coefficient in Eq. (2)
ω''	Coefficient in Eq. (2)
$\|p\|$	Amplitude of wave-induced pore pressure
ΔV	Volume compression of the porous seabed
ΔV_s	Volume compression of the soil skeleton
ΔV_p	Volume compression of the pore-fluid

Table 1
Typical theoretical models for wave-induced transient pore pressure in a seabed under various assumptions.

Three categories	Basic assumptions		Governing equations	Literatures
	Soil-skeleton	Pore-fluid		
(1) RS-IF seabed	Isotropic, rigid, finite thickness	Incompressible	Laplace equation	Putnam (1949)
	Isotropic, rigid, infinite thickness	Incompressible	Laplace equation	Reid and Kajirua (1957)
(2) RS-CF seabed	Isotropic, rigid, finite thickness	Compressible	Diffusion equation	Moshagen and Tørum (1975)
(3) ES-CF seabed	Isotropic, elastic, infinite thickness	Compressible	Biot's consolidation equation	Yamamoto et al. (1978); Okusa (1985)
	Anisotropic, elastic, infinite thickness	Compressible	Biot's consolidation equation	Madsen (1978)
	Anisotropic, elastic, finite thickness	Compressible	Biot's consolidation equation	Hsu and Jeng (1994); Jeng and Hsu (1996)

Yamamoto et al. (1978), termed as "Yamamoto solution" thereafter) have been widely employed for evaluating the excess pore pressure responses in a non-cohesive seabed. If the relevant assumptions for the RS-CF or the RS-IF seabed are adopted (see Table 1), Yamamoto solution for the pore pressure responses in an ES-CF seabed can be degenerated into the other models correspondingly. It should be noted that, no phase-lag can be predicted under the assumptions of a RS-IF seabed; whereas the phase-lag increases linearly with the soil depth under the assumptions of a RS-CF seabed. According to Yamamoto solution, the pore pressure responses are closely related to both the wave parameters and the soil properties.

Although it has been recognized that the amplitude-attenuation could be accompanied by a phase-lag, previous studies predominantly focused on the amplitude-attenuation of transient pore pressures. Until now, little attention has been paid to the accompanied phase-lag phenomenon. As reported by Yamamoto et al. (1978), the amplitude-attenuation of pore pressures became more remarkable for smaller wave period of progressive waves. It was observed that a significant phase-lag can be generated in a fine-sand bed, while no phase-lag occurred in a coarse-sand bed. Recently, Liu et al. (2015) physically simulated the transient pore pressure responses in a sandy deposit under the one-dimensional quasi-standing wave condition by employing a cylinder equipment. Their results further indicated that the pore pressure amplitude at a certain soil depth would increase with increasing wave period, wave height, soil permeability or soil saturation; the values of phase-lag could be up to approximately $2\pi/3$ in their examined loose-sand sample with low saturation. Despite previous efforts on phenomenological observations, the theoretical characterizations for both the amplitude-attenuation and the phase-lag of wave-induced pore pressure have not been well achieved. Meanwhile, their correlations need to be further established for a better understanding the whole scenario of the spatial and temporal distributions of transient pore pressures in a porous seabed.

In the present study, a series of flume tests were firstly conducted to observe the spatial and temporal distributions of transient pore pressures in a fine-sand bed and a medium-sand bed, respectively. The

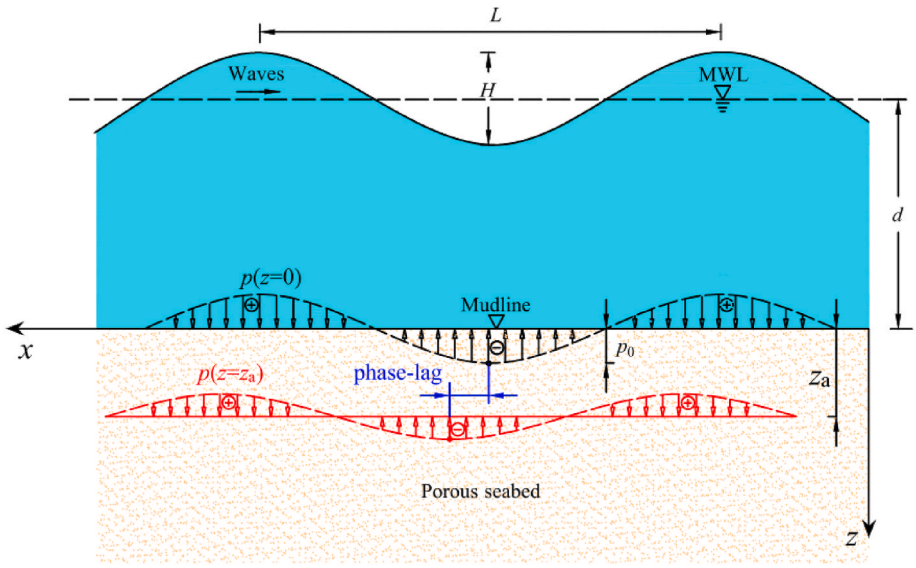

Fig. 1. Illustration of transient pore pressure under progressive waves: phase-lag and amplitude-attenuation (H: wave height; L: wave length; d: water depth; z: soil depth; z_a: an arbitrary soil depth; MWL: mean water line).

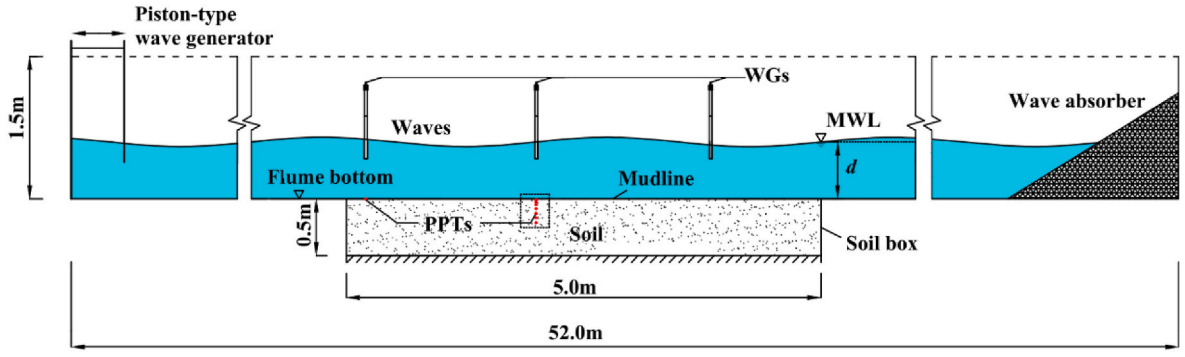

Fig. 2. Experimental set-up for wave-induced pore pressure in a sand-bed (d: water depth).

explicit expressions for the amplitude-attenuation and the phase-lag were then derived, which were compared and validated with the experimental data. Parametric studies were further made to examine the effects of main influential parameters. Moreover, the spatio-temporal correlation of transient pore pressures is finally established.

2. Flume observations

As illustrated in Fig. 1, when ocean waves propogating over a porous seabed, the excess pore pressure can be induced in the soil. The amplitude of the pore pressure attenuates with the increase of soil depth. Meanwhile, there always exists a phase-lag between the wave pressure at the mudline ($z = 0$) and the excess pore pressures at certain depth of the seabed (e.g., $z = z_a$, see Fig. 1).

2.1. Experimental set-up and test procedures

A series of wave-soil interaction tests was conducted in a large wave flume of 52.0 m (length) × 1.0 m (width) × 1.5 m (depth) (see Fig. 2) at Institute of Mechanics, Chinese Academy of Sciences. In the middle of the flume, a soil box of 5.0 m (length) × 1.0 m (width) × 0.5 m (depth) was constructed. A piston-type wave generator was installed at the inlet of the flume for generating progressive waves. At the end of flume, a beach-type wave absorber was used, whose wave reflection coefficient is generally less than 5.0%. Several miniature pore pressure transducers (PPTs) were utilized to measure the wave-induced pore pressure in the soil as well as the pressure fluctuation at the flume bottom. The probe of the PPT is 5.0 mm in diameter and 17.0 mm in length, with the measuring range of 0–20 kPa and accuracy of 0.2%. Meanwhile, three wave gauges (WGs) were also employed to simultaneously monitor the free water surface elevation.

Two typical sand–beds were employed in this study, i.e. fine-grained sand (fine sand) and medium-grained sand (medium sand), whose grain size distributions are given in Fig. 3. The main physical properties of the sands and the wave parameters adopted in the physical modeling are summarized in Table 2.

The following test procedures were adopted:

(1) Installation of pore pressure transducers in the wave flume:

The wave flume and the centrally located soil box were firstly emptied and cleaned. Eight miniature pore pressure transducers (PPTs) were employed, whose argil-covers were deaired before their installations. Under the wave gauge (WG), the PPTs were installed at various depths in the fine sand ($z = 0$, 1.0 cm, 3.0 cm, 6.0 cm, 10.0 cm, 15.0 cm, 20.0 cm) and the medium sand ($z = 0$, 3.0 cm, 12.0 cm) with the support of fixing racks.

(2) Sandbed preparation with sand-raining technique:

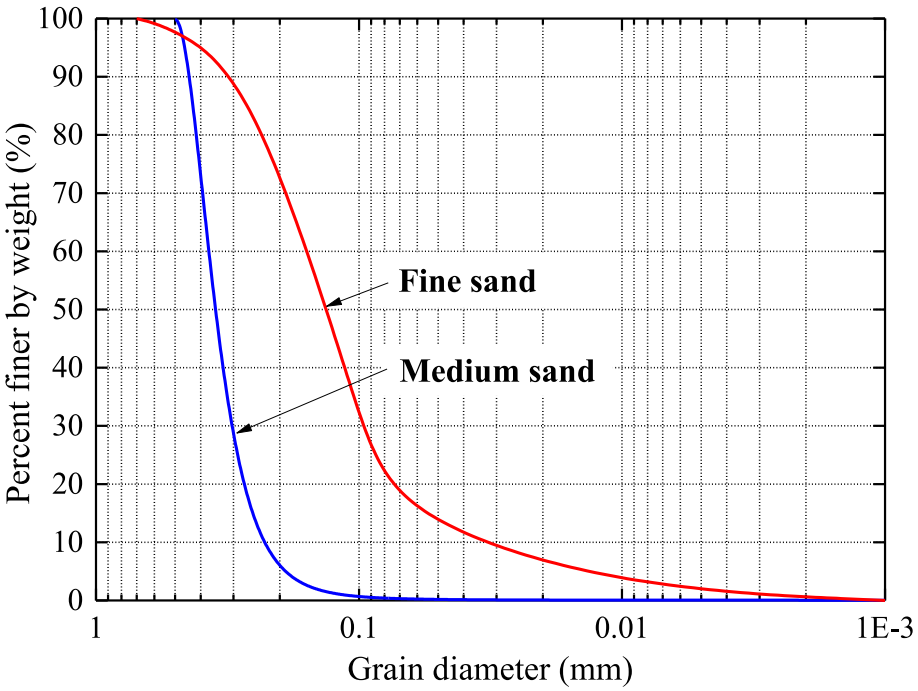

Fig. 3. Grain size distributions of the medium sand and the fine sand.

Table 2
Wave parameters and soil properties in the flume experiments.

Wave parameters:	Symbols (units)	Values	Values
Water depth	d (m)	0.5	0.5
Wave period	T (s)	1.2–1.8	1.2
Wavelength	L (m)	2.05–3.57	2.05
Wave height	H (m)	0.130	0.095
Soil properties:		Fine sand	Medium sand
Mean size of grains	d_{50} (mm)	0.12	0.38
Effective size of grains	d_{10} (mm)	0.03	0.23
Buoyant unit weight	γ' (N/m^3)	9.70×10^3	9.06×10^3
Coefficient of permeability	k_s (m/s)	9.60×10^{-5}	1.88×10^{-4}
Degree of saturation	S_r	0.993	0.993
Porosity	n	0.40	0.44
Relative density	D_r	0.62	0.35
Shear modulus	G (Pa)	23.8×10^6	20.2×10^6
Poisson's ratio	ν	0.30	0.27
Depth of the soil box in the flume	d_s (m)	0.5	0.5

The sand-bed was carefully prepared by employing sand-raining technique, i.e., the dry sand particles in a reciprocating trolley were rained into the clean water in the soil box. Such sand-raining technique can efficiently ensure the sand-beds are generally homogenious and quasi-saturated. The surface of the sand-bed was then leveled off smoothly with a scraper, and the wave flume was slowly filled with water to a given depth (e.g., $d = 0.5$ m). The relative density of the sand-bed (D_r) was verified with $D_r = (e_{max} - e)/(e_{max} - e_{min})$, where e_{max} and e_{min} are the maximum and the minimum void ratio of the sand, respectively; e is the void ratio under the in-situ condition after deposition, which was obtained by traditional test method for drying the saturated sand samples in an oven (Knappett and Craig, 2012). Note: the water depth was kept constant during the physical modeling.

(3) Simultaneous measurement of wave surface elevation and excess pore pressures:

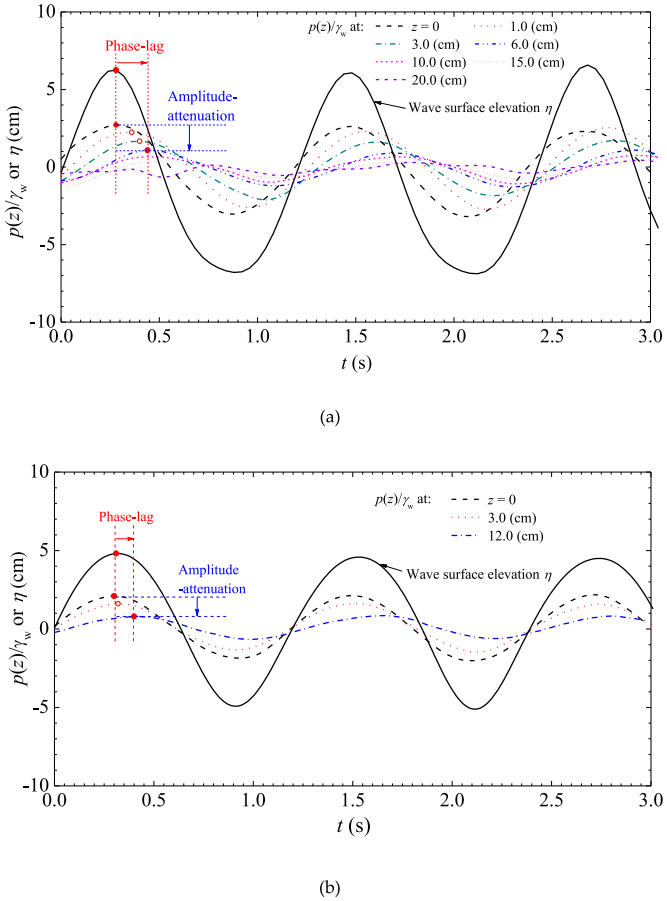

Fig. 4. Typical time series of the wave surface elevation η and the corresponding $p(z)/\gamma_w$ at various depths in the sand-beds ($T = 1.2$ s): (a) fine sand; (b) medium sand.

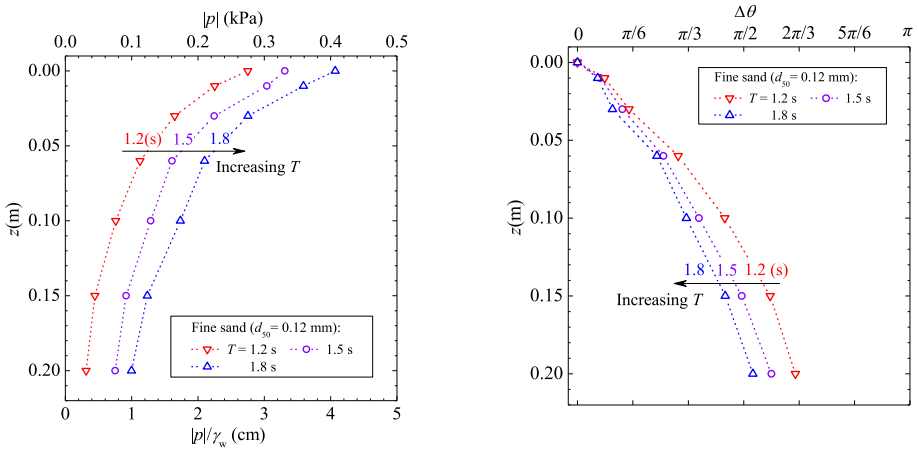

Fig. 5. Wave-induced transient pore pressure in the fine sand (d_{50} = 0.12 mm): (a) amplitude-attenuation: $|p|$ vs. z; and (b) phase-lag: $\Delta\theta$ vs. z.

The wave maker was then activated and the progressive waves were generated. Meanwhile, the multichannel synchronous sampling system was started to simultaneously measure the free surface elevation of progressive waves and excess pore pressures in the sand-bed with WGs and PPTs, respectively.

2.2. Test results

The measured wave surface elevation and the corresponding pore pressure responses at several selected soil depths in the fine sand and in the medium sand are shown in Fig. 4 (a) and (b), respectively. In these figures, η and $p(z)$ denote the wave surface elevation and the wave-induced pore pressure at the soil depth z, respectively. For the purpose of comparison, the expression $p(z)/\gamma_w$ is used to keep the same unit with η, where γ_w is the unit weight of water ($\gamma_w = 9.8 \times 10^3 \mathrm{N/m^3}$). As shown in these figures, both the wave surface elevation and the corresponding transient pore pressures are featured with quasi-sinusoidal oscillations. The wave-induced pore pressure at the seabed surface ($z = 0$) had the same phase with the wave surface elevation (η). In addition to the amplitude-attenuation, an evident phase–lag of the transient pore pressures with increasing soil depth was also identified by the simultaneous measurements in the examined fine sand (Fig. 4(a)) and the medium sand (Fig. 4(b)), respectively. When comparing the transient pore pressures at soil depth z = 3.0 cm between Fig. 4(a) and (b), one can identify that the amplitude-attenuation and phase-lag were more significant in the fine-sand bed than in the medium-sand bed.

The amplitude-attenuation of transient pore pressure responses in the sand-beds for various wave periods and the corresponding phase-lag of the transient pore pressure are examined (see Fig. 5(a) – (b)). As shown in Fig. 5(a), the progressive waves with larger wave period (T) induced higher pore pressure amplitude ($|p|$) at the mudline, which attenuated exponentially with the increase of soil depth (z). It is indicated that the vertical gradient of the pore-pressure amplitudes decreased with increasing soil depth. In other words, the pore-pressure amplitudes attenuated more significantly in the shallower layer of the bed. Such phenomena have been intensively investigated in previous studies (see Sumer, 2014; Jeng, 2018). In this study, the corresponding phase-lag ($\Delta\theta$) of the transient pore pressue was further detected simultaneously (see Fig. 5(b)). In Fig. 5 (b), the phase-lag of the transient pore pressure was obtained with $\Delta\theta = 2\pi(\Delta T/T)$, where ΔT is the time-lag between the regular waves and the corresponding excess pore pressure. For a given soil depth (z), the values of $|p|$ increased with increasing wave period T from 1.2 s to 1.8 s (Fig. 5(a)); nevertheless, with the increase of T, the values of $\Delta\theta$ decreased, i.e., the phase-lag was weaken (slowed down) at the deeper soil layer (Fig. 5(b)).

Fig. 6(a) – (b) show the variations of amplitude-attenuation $|p|/p_0$

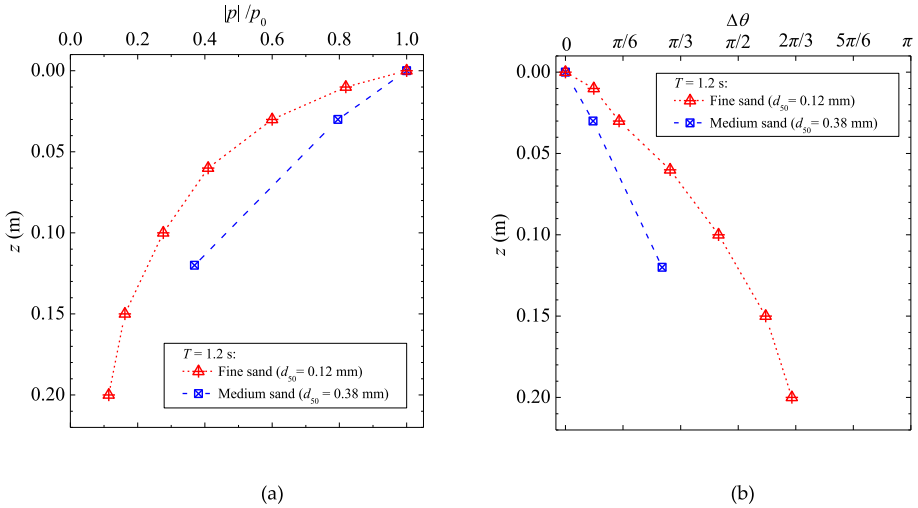

Fig. 6. Variations of (a) amplitude-attenuation $|p|/p_0$ and (b) phase-lag $\Delta\theta$ with z (T = 1.2 s): Comparisons between the fine sand and the medium sand.

and phase-lag $\Delta\theta$ with z for $T = 1.2$ s. In these figures, the experimental results between the fine sand and the medium sand are compared. The ratio "$|p|/p_0$" denotes the relative magnitude of the pore pressure amplitude at a certain soil depth $|p|$ ($z > 0$) to that at the mudline p_0 ($z = 0$). As shown in Fig. 6(a)–(b), both the amplitude-attenuation and the phase-lag got much more significant with z in the fine sand-bed than in the medium sand-bed.

The above observations indicated that the amplitude-attenuation and the phase-lag in a non-cohesive seabed could be closely correlated, which motivated the authors to further deliberate how to quantitatively characterize them.

3. Analytical characterization for amplitude-attenuation and phase-lag

3.1. Derivations

On the basis of Biot's theory framework for porous elastic media (Biot, 1941), an analytical solution for wave-induced pore pressure in a porous seabed was ever derived by Yamamoto et al. (1978). The basic assumptions were adopted as follows (Yamamoto et al., 1978): (1) The seabed is reagrded as an infinite, isotropic and homogeneous poro-elastic medium, and the soil skeleton obeys Hooke's law. (2) The pure water without gas bubbles is generally assumed to be incompressible; but the actual pore-fluid in the soil may contain a limited content of bubbles, which would make the pore-fluid compressible. (3) The seepage of pore-fluid obeys Darcy's law. A brief introduction for the derivation of the Yamamoto solution can be referenced in Qi and Gao (2018).

The wave-induced oscillatory pore pressure $p(z)$ can be expressed as (Yamamoto et al., 1978):

$$p(z) = P_b[(1-\alpha)\exp(-\lambda z) + \alpha\exp(-\lambda' z)] \tag{1}$$

where $P_b = p_0\exp[i(\lambda x + \omega t)]$ is the wave pressure fluctuation at the seabed surface ($z = 0$, see Fig. 1), in which $p_0 = 0.5\gamma_w H/\cosh(\lambda d)$ is the amplitude of P_b; the variables α and λ' can be calculated with Eqs. (2) and (3):

$$\alpha = \frac{im\omega''}{(1-\lambda'/\lambda) + i(1+m)\omega''} \tag{2}$$

$$(\lambda')^2 = \lambda^2 + i\frac{\gamma_w}{k_s}\omega\left(\frac{1-2\nu}{2(1-\nu)G} + \frac{n}{K'}\right) \tag{3}$$

where $m = nG/(K'(1-2\nu))$, in which the soil porosity $n = e/(1+e)$, e is the void ratio, K' is the apparent bulk modulus of the pore-fluid, G and ν are the shear modulus and the Poisson's ratio of the soil, respectively; $\omega'' = \beta(\omega'/\lambda^2)$, in which $\beta = (1-\nu)/(1-2\nu)$, $\omega' = \omega/c$, ω ($=2\pi/T$) is the angular frequency of the waves, $c = \frac{k_s}{\gamma_w}/\left(\frac{n}{K'} + \frac{1-2\nu}{2(1-\nu)G}\right)$; and "$i$" denotes the imaginary part of a complex number.

Eqs. (1)–(3) indicate that wave-induced pore pressure $p(z)$ is mainly related to the following wave parameters (λ, ω, H, d, and γ_w) and soil properties (n, K', G, ν and k_s). Note that the above wave parameters are not independent. Essential for gravitational water waves is that free propagating waves of non-zero amplitude only exist when the angular frequency ω and the wave number λ ($= 2\pi/L$, in which L is the wavelength) satisfy the dispersion relationship (see Sarpkaya, 2010):

$$\omega^2 = g\lambda\tanh(\lambda d) \tag{4}$$

For the boundary-value problem of wave-seabed interactions, the soil layer with significant transient pore pressure responses (e.g., $z \approx 0.10$ (m) in the present flume tests, see Fig. 5(a)) is generally much shorter than the wavelength ($L \approx 2.05$ (m), see Table 2), i.e., $z/L \ll 1.0$. The transient pore pressure under wave troughs can be essentially regarded as a quasi-one-dimensional (quasi-1D) process, during which the upward seepage can be generated by pore pressure gradients. The soil compressibility for a poro-elastic seabed under such quasi-1D condition is discussed in more details in Appendix A. Substituting Eq. (A2) to Eq. (A1), one can express the apparent longitudinal bulk modulus of poro-elastic media (K) as follows:

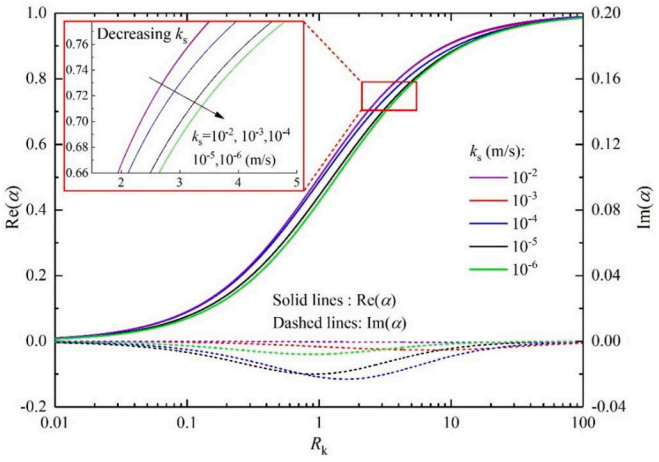

Fig. 7. Variations of Re(α) and Im(α) with R_k for various values of k_s ($d = 0.5$ m, $T = 1.2$ s; $G = 23.8$ MPa, $\nu = 0.30$, $n = 0.40$).

$$K\left(=\left(\frac{1}{M} + \frac{n}{K'}\right)^{-1}\right) = \left(\frac{1-2\nu}{2(1-\nu)G} + \frac{n}{K'}\right)^{-1} \tag{5}$$

To quantitatively characterize the relative rigidity of soil-skeleton to pore-fluid, the parameter R_k is introduced, i.e.

$$R_k\left(=\frac{nM}{K'}\right) = \frac{2n(1-\nu)G}{(1-2\nu)K'} \tag{6}$$

Eq. (6) indicates that, in addition to G/K', the soil porosity (n) and Poisson's ratio (ν) should also be involved to characterize soil compressibility. $R_k = 1.0$ denotes the rigidity of soil-skeleton and that of pore-fluid are equivalent. If $R_k \ll 1.0$, then $K \approx M$; and if $R_k \gg 1.0$, then $K \approx K'/n$.

Considering the expression of K with Eq. (5), Eq. (3) can be further simplified as

$$(\lambda')^2 = \lambda^2 + \frac{\omega\gamma_w}{Kk_s}i \tag{7}$$

As λ' is a complex number, we assume

$$\lambda' = \xi_1 + \xi_2 i \tag{8}$$

In which both ξ_1 and ξ_2 are real numbers. Substituting Eq. (8) into Eq. (7), one can obtain the expressions of ξ_1 and ξ_2, respectively:

$$\xi_1 = \frac{\sqrt{2}}{2}\left(\lambda^2 + \sqrt{\lambda^4 + \left(\frac{\omega\gamma_w}{Kk_s}\right)^2}\right)^{1/2} \tag{9a}$$

$$\xi_2 = \frac{\sqrt{2}}{2}\left(-\lambda^2 + \sqrt{\lambda^4 + \left(\frac{\omega\gamma_w}{Kk_s}\right)^2}\right)^{1/2} \tag{9b}$$

Substituting Eqs. (8), (9a)–(9b) into Eq. (2), the complex number α can then be explicitly expressed as a real part (Re(α)) and an imaginary part (Im(α)), respectively, i.e.,

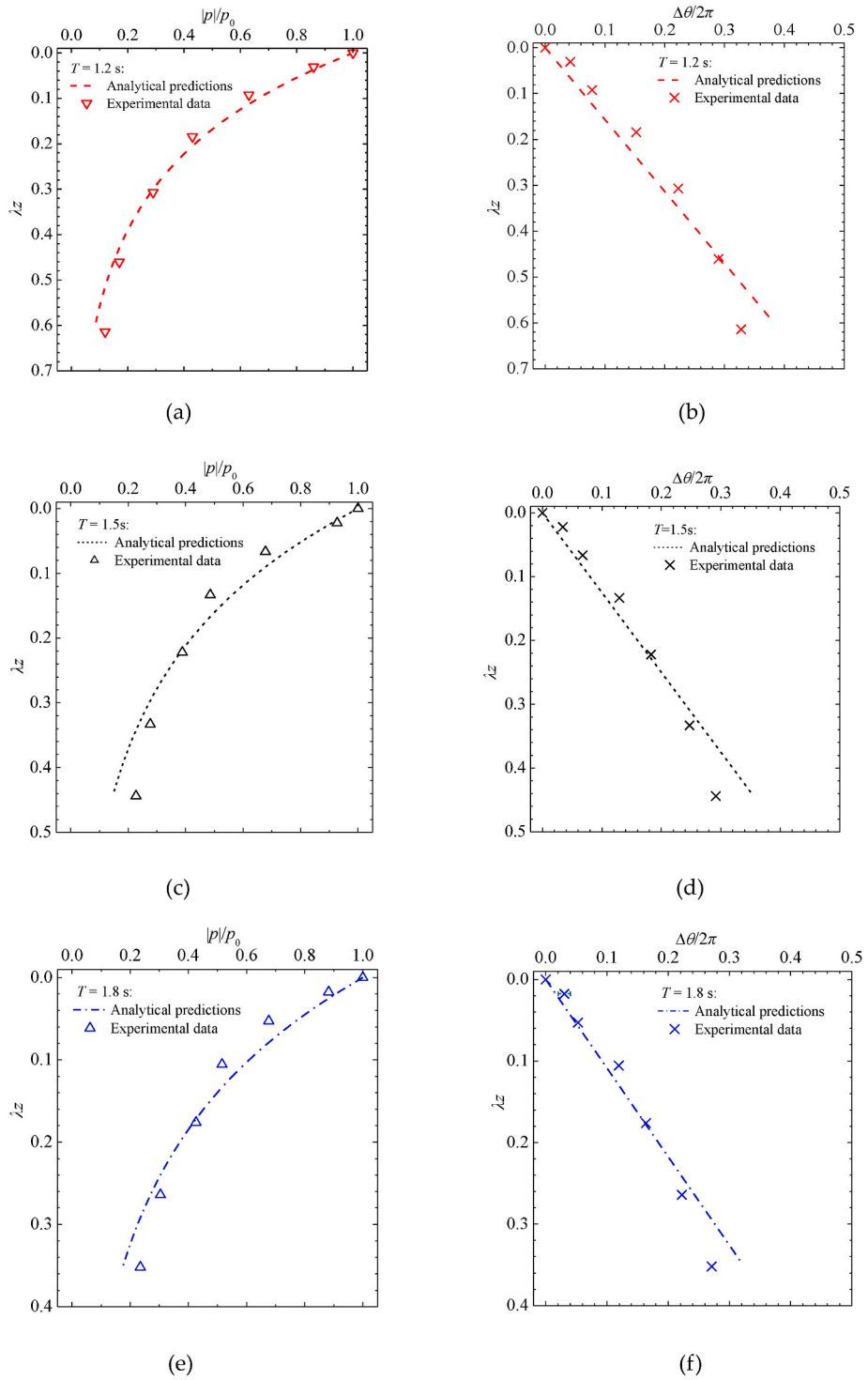

Fig. 8. Comparisons of amplitude-attenuation $|p|/p_0$ and phase-lag $\Delta\theta/2\pi$ in the fine-sand bed (d_{50} = 0.12 mm) between analytical predictions and experimental data: (a)–(b): T = 1.2 (s); (c)–(d): T = 1.5 (s); (e)–(f): T = 1.8 (s).

$$\alpha = \mathrm{Re}(\alpha) + \mathrm{Im}(\alpha)i = \frac{m\omega''\left((1+m)\omega'' - \frac{\xi_2}{\lambda}\right) + m\omega''\left(1 - \frac{\xi_1}{\lambda}\right)i}{\left(1 - \frac{\xi_1}{\lambda}\right)^2 + \left((1+m)\omega'' - \frac{\xi_2}{\lambda}\right)^2} \tag{10}$$

On the basis of Eq. (10), the variations of α with the relative compressibility parameter R_k for various values of the permeability coefficient k_s can be obtained, as shown in Fig. 7. In this figure, both real part (Re(α)) and imaginary part (Im(α)) of α are provided, respectively. The wave parameters and soil properties are set as: d = 0.5 (m), T = 1.2 (s); G = 23.8 (MPa), ν = 0.30, n = 0.40; k_s = 10^{-2}–10^{-6} (m/s). As indicated in Fig. 7, with R_k increasing from 10^{-2} to 10^{2}, the values of Re (α) increase nonlinearly from approximately 0 to 1.0. The absolute values of Re(α) are much larger than those of Im(α), especially for R_k > 1.0. In comparison with the relative rigidity R_k, the soil permeability has slight effect on the values of α for the examined wide range of k_s (= 10^{-2}–10^{-6} (m/s)).

It is interesting to further investigate two limiting cases of R_k, i.e., (1)

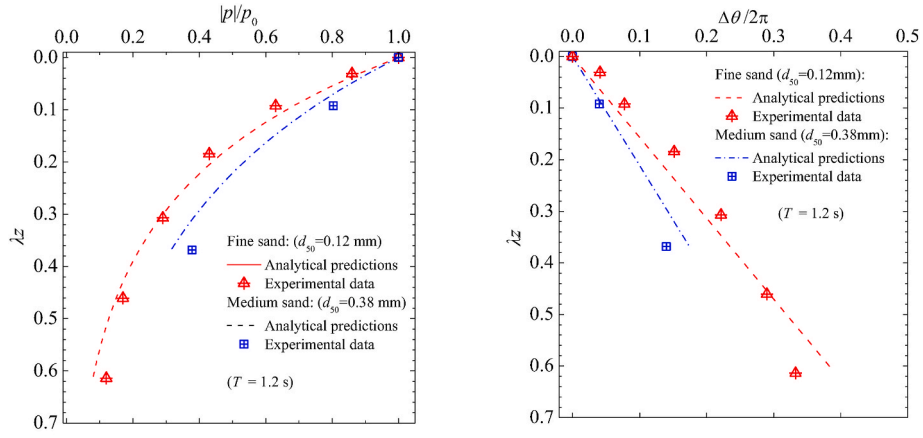

(a) (b)

Fig. 9. Comparisons of (a) amplitude-attenuation $|p|/p_0$ and (b) phase-lag $\Delta\theta/2\pi$ between the results for the fine sand and those for the medium sand ($T = 1.2$ s).

$R_k \ll 1.0$ and (2) $R_k \gg 1.0$, respectively:

(1) Case-I: $R_k \ll 1.0$

For the case of $R_k \ll 1.0$ ($R_k \sim O(10^{-2})$ or less), the compressibility of pore-fluid is much smaller than that of soil-skeleton, e.g., the seabed soil is fully-saturated. Then, the variable α would approach zero (i.e., $\alpha \to 0$, see Fig. 6). The solution for wave-induced pore pressure (Eq. (1)) can thereby be simplified as

$$p(z) \approx p_0 \exp(-\lambda z)\exp[i(\lambda x + \omega t)] \quad (for\ R_k \ll 1.0) \tag{11}$$

i.e., the amplitude-attenuation:

$$\frac{|p|}{p_0} \approx \exp(-\lambda z) \quad (for\ R_k \ll 1.0) \tag{11a}$$

As indicated by Eq. (11) or (11'), if $R_k \ll 1.0$, the amplitude-attenuation of transient pore pressure in the seabed would be mainly related to the wave number (λ) and independent of soil properties. That is, the amplitude of oscillatory pore pressure would attenuate exponentially with soil depth (also see Yamamoto et al., 1978). Moreover, the phase-lag phenomenon would not occur under such condition.

(2) Case-II: $R_k \gg 1.0$

Similarly, if $R_k \gg 1.0$ ($R_k \sim O(10^2)$ or more), the compressibility of pore-fluid is much larger than that of soil–skeleton, e.g., some content of air or gas is entrapped within the pores of soil. The variable α would then approach 1.0 (i.e., $\alpha \to 1.0$, see Fig. 6), and Eq. (1) can be further simplified as

$$p(z) \approx p_0 \exp(-\lambda' z)\exp[i(\lambda x + \omega t)] \quad (for\ R_k \gg 1.0) \tag{12}$$

Substituting Eq. (8) into Eq. (12) and denoting the phase of progressive waves $\theta = \lambda x + \omega t$, one can derive

$$p(z) \approx p_0 \exp(-\xi_1 z)\exp[i(\theta - \xi_2 z)] \quad (\text{for } R_k \gg 1.0) \tag{12a}$$

in which, the two variables ξ_1 and ξ_2 (real numbers) can be calculated with Eqs. (9a) and (9b), respectively. Eq. (12') indicates that, unlike Case-I, the amplitude-attenuation of $p(z)$ with soil depth (z) would be mainly related to the variable ξ_1, i.e.

$$|p|/p_0 \approx \exp(-\xi_1 z) = \exp\left(-\frac{z\sqrt{2}}{2}\left(\lambda^2 + \sqrt{\lambda^4 + \left(\frac{\omega\gamma_w}{Kk_s}\right)^2}\right)^{1/2}\right) \quad (for\ R_k \gg 1.0) \tag{13}$$

Furthermore, the explicit expression for the phase-lag ($\Delta\theta$) of the transient pressure can be obtained as

$$\Delta\theta(=\xi_2 z) = \frac{z\sqrt{2}}{2}\left(-\lambda^2 + \sqrt{\lambda^4 + \left(\frac{\omega\gamma_w}{Kk_s}\right)^2}\right)^{1/2} \quad (for\ R_k \gg 1.0) \tag{14}$$

As indicated by Eqs. 13 and 14, if $R_k \gg 1.0$, the amplitude of oscillatory pore pressure would also attenuate exponentially with soil depth; the phase-lag would increase linearly with soil depth. Since the values of

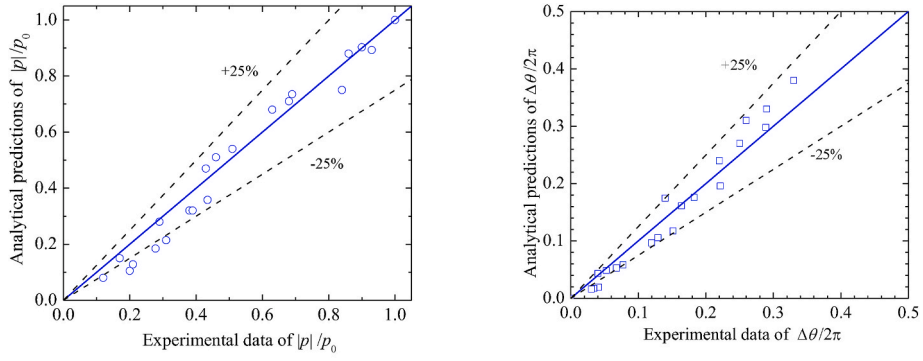

(a) (b)

Fig. 10. Comparisons of (a) amplitude-attenuation $|p|/p_0$ and (b) phase-lag $\Delta\theta/2\pi$ between analytical and experimental results.

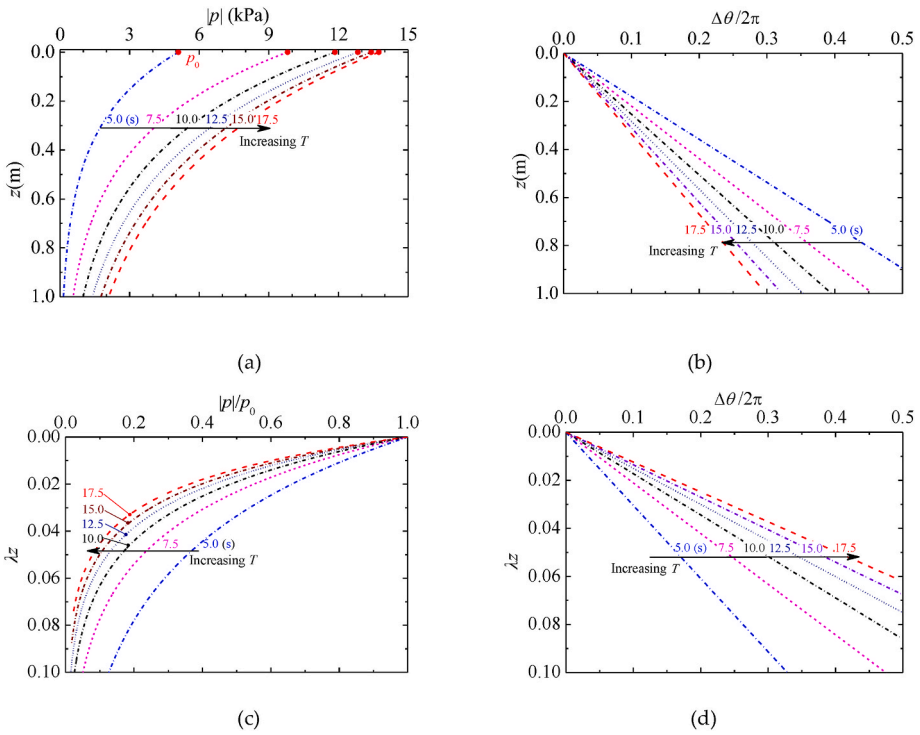

Fig. 11. Effects of wave period (T) on amplitude-attenuation and phase-lag: (a) $|p|$ vs. z; (b) $\Delta\theta/2\pi$ vs. z; (c) $|p|/p_0$ vs. λz; (d) $\Delta\theta/2\pi$ vs. λz ($R_k = 15.0$, $Kk_s \approx 500\ \mathrm{Nm^{-1}s^{-1}}$).

ξ_1 are generally larger than wave number (i.e. $\xi_1 > \lambda$, see Eq. (9a)), the amplitude-attenuation in the seabed would be more significant compared with that in Case-I.

For a moderate magnitude of R_k (e.g., $10^{-1} < R_k < 10$, see Fig. 6), the explicit expression for the phase-lag $\Delta\theta$ is algebraically cumbersome; nevetheless, the values of $\Delta\theta$ can be evaluated in between "zero" (for Case-I) and "$\xi_2 z$" (see Eq. (13), for Case-II). Correspondingly, the amplitude-attenuation $|p|/p_0$ would fall between "$\exp(-\lambda z)$" (see Eq. (11), for Case-I) and "$\exp(-\xi_1 z)$" (see Eq. (12), for Case-II).

3.2. Comparisons with flume observations

In this section, the analytical predictions with the derived solutions are compared with the wave flume data. Submitting the values of the soil properties listed in Table 2 into Eq. (6), the values of R_k for the fine-sand and the medium-sand bed can be obtained as $R_k = 47.6$ and 40.3, respectively. As $R_k \gg 1.0$ for the examined two typical sands (Case-II), the amplitude-attenuation and phase-lag can be evaluated with Eqs. (13) and (14), respectively.

To verify the analytical solutions in Section 3.1, the comparisons of the vertical distributions of amplitude–attenuation ($|p|/p_0$) and phase–lag ($\Delta\theta/2\pi$) between the analytical predictions and the present experimental data are presented in Fig. 8(a)–(f) in the fine sand for the wave period $T = 1.2$ (s), 1.5 (s) and 1.8 (s), respectively. In Fig. 8, the non-dimensional soil depth "λz" characterizes the relative magnitude of the soil depth (z) to the wavelength (L), which is a key combined parameter in the analytical solutions (see Section 3.1). Fig. 9(a) and (b) show the comparisons between the results for $T = 1.2$ (s) in the fine sand and those in the medium sand. The comparisons of $|p|/p_0$ and $\Delta\theta/2\pi$ between all of the measured experimental data in Fig. 5(a) and (b) and the corresponding analytical predictions are shown in Fig. 10 (a) and (b), respectively. It is indicated that the analytical and experimental results generally match well with each other, i.e., most of the data lie within ±25% error range.

Certain deviations of the analytical predictions from the test data still exist, especially in the deeper soil layer with larger values of λz (see Fig. 8). This could be attributed to the bottom boundary effect from the soil box in the wave flume. As implied in the numerical simulations by Gao (2003), for a sand-bed of finite thickness (e.g., $d_s/L = 0.14$ for $T = 1.8$ s), the amplitude-attenuation would slow down when $\lambda z > 0.26$ (see Fig. 8 (e)); meanwhile, the phase-lag also slowed down as shown in Fig. 8 (f). With increasing wave period (the wavelength is enlarged correspondingly), the bottom boundary effect on pore-pressure distributions in the soil box with a rigid impermeable bottom (Fig. 2) would get non-negligible (see Hsu and Jeng, 1994).

It should be noted that the present wave flume experiments for the validation of the derived explicit solutions are under the shallow water condition. With increasing water depth (d), the absolute pore water pressure (P_0) would increase, which can further raise the apparent bulk modulus of the pore–fluid (K') (see Eq. (A3)). If the degree of saturation (S_r) and the porosity (n) of the soil are kept unchanged, the values of the apparent bulk modulus K (see Eq. (5)) would increase accordingly; meanwhile, the amplitude of wave pressure fluctuations at the seabed surface would correspondingly decrease. To well understand the spatio-temporal distributions of wave-induced pore pressure, a parametric study will be conducted in Section 4.

4. Parametric analyses

From the explicit expressions for the amplitude-attenuation (Eq. (13)) and the phase-lag (Eq. (14)), one can recognize that the spatial and temporal distributions of wave-induced pore pressure are predominantly related to the wave number "λ" and the angular frequency "ω" (or wave period T), and a combined rigidity-permeability parameter "Kk_s" of the seabed soil.

In this section, parametric analyses are conducted to examine the effects of these influential parameters on the phase–lag and the amplitude–attenuation. As a case study, the wave parameters are set as follows: water depth $d = 10.0$ (m), wave height $H = 3.0$ (m), the values of wave period T are various in Section 4.1; the degree of saturation is set as $S_r = 0.956$, the other soil properties (including k_s, G, n and ν) are same with those of the fine sand in the present flume experiments (see

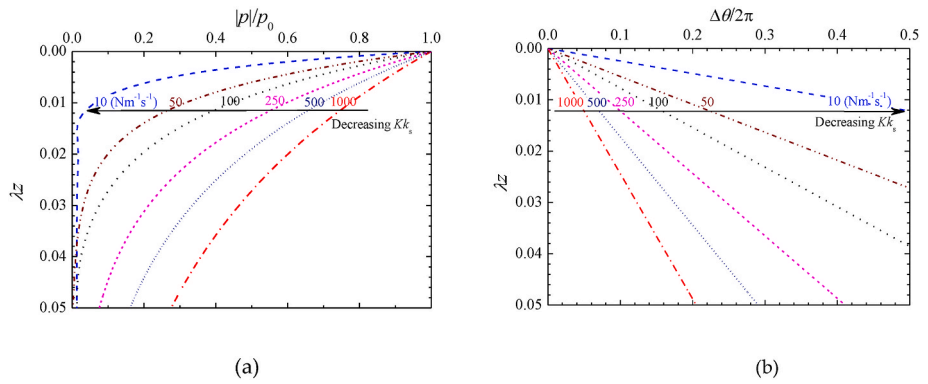

Fig. 12. Effects of the combined soil rigidity-permeability parameter Kk_s on (a) the amplitude-attenuation and (b) the phase-lag of wave-induced transient pore pressures ($R_k \gg 1.0$, $T = 10.0$ s).

Table 2).

4.1. Effects of wave period

As aformentioned in Section 3.2, the relative compressibility of the examined fine sand R_k can be evaluated with Eq. (6), i.e., $R_k \approx 15.0$; the apparent longitudinal bulk modulus K can be calculated with Eq. (5), and the corresponding $Kk_s \approx 500$ ($Nm^{-1}s^{-1}$). As $R_k \gg 1.0$, the amplitude-attenuation and the phase-lag can be predicted with Eqs. (13) and (14), respectively. In the parametric study, the values of wave period are various: $T = 5.0$, 7.5, 10.0, 12.5, 15.0 and 17.5 (s), i.e. the corresponding values of $\lambda = 0.170$, 0.096, 0.068, 0.053, 0.044 and 0.037 (m^{-1}), respectively. Note that the two wave parameters λ and T (or ω) are correlated by the dispersion relationship (see Eq. (4)).

The vertical distributions of amplitude-attenuation and phase-lag in the soil for various values of the wave period are shown in Fig. 11. Similar to the results of the flume tests (see Fig. 5), for a given soil depth (z), the values of $|p|$ increase as the wave period increasing from $T = 5.0$ (s) to 17.5 (s) (see Fig. 11(a)), and the values of phase-lag $\Delta\theta/2\pi$ decrease with increasing T (see Fig. 11(b)). Nevertheless, in the non-dimensional forms $|p|/p_0$ vs.λz, the values of $|p|/p_0$ decrease with increasing T for a given value of λz (see Fig. 11(c)); Correspondingly, the values of phase-lag $\Delta\theta/2\pi$ increase with increasing T (see Fig. 11(d)).

4.2. Effects of seabed properties: combined soil rigidity-permeability parameter Kk_s

As indicated by Eqs. 13 and 14, both phase-lag and amplitude-attenuation are influenced by the rigidity and permeability of the seabed soil with a combined soil parameter "Kk_s" under the condition of $R_k \gg 1.0$. For non-cohesive soils, the values of permeability coefficient (k_s) may vary from 10^{-6} m/s (for a very-fine or silty sand) to 10^{-2} m/s (for a coarse sand); and the values of shear modulus (G) may vary from 1.0×10^6 Pa (soft silt) to 5.0×10^8 Pa (very-dense sand). The evaluation and influential factors for the rigidity and permeability of a porous seabed can be referenced in Appendix A. To investigate the effects of seabed properties on the spatial and temporal distributions of transient pore pressures, a wide range of the combined soil rigidity–permeability parameter Kk_s (from 10 $Nm^{-1}s^{-1}$ to 1000 $Nm^{-1}s^{-1}$) is examined.

The amplitude-attenuation and the phase-lag of wave–induced transient pore pressures for various values of Kk_s are shown in Fig. 12(a) and (b), respectively. As indicated by Fig. 12(a), for a given value of λz, the amplitude-attenuation $|p|/p_0$ drops dramatically with deceasing Kk_s from 10^3 $Nm^{-1}s^{-1}$ to 10 $Nm^{-1}s^{-1}$. That is, the more rigid or/and permeable the soil is, the more deeply the wave pressure can be transmitted down into the seabed. Meanwhile, the phase-lag gets more significant for smaller values of Kk_s (see Fig. 12 (b)).

5. Spatio-temporal correlation of transient pore pressures

In this section, dimensional analyses are further made for analytically characterizing the spatio-temporal correlation of transient pore pressures in the seabed under waves. Eq. (7) can be re-expressed in dimensionless forms, i.e.

$$\left(\frac{\lambda'}{\lambda}\right)^2 = 1 + i\frac{\omega\gamma_w}{Kk_s\lambda^2} \tag{15}$$

A non-dimensional parameter (I_c) can herein be introduced:

$$I_c = \frac{\omega\gamma_w}{Kk_s\lambda^2} \tag{16}$$

which is a combination of both wave parameters (λ ω) and soil properties (k_s, K). Eq. (15) can be further written as

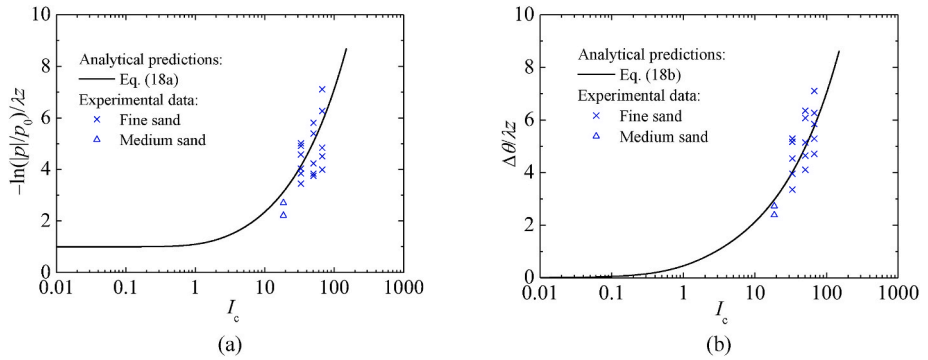

Fig. 13. Comparisons of the variations of (a) amplitude-attenuation and (b) phase-lag with I_c between analytical results and experimental data.

$$\left(\frac{\lambda'}{\lambda}\right)^2 = 1 + iI_c \tag{15a}$$

Considering the expression of I_c with Eq. (16), Eqs. (9a) and (9b) can be expressed as following dimensionless forms, respectively:

$$\frac{\xi_1}{\lambda} = \left(\frac{\sqrt{1+I_c^2}+1}{2}\right)^{1/2} \tag{17a}$$

$$\frac{\xi_2}{\lambda} = \left(\frac{\sqrt{1+I_c^2}-1}{2}\right)^{1/2} \tag{17b}$$

Substituting Eqs. (17a) – (17b) into Eqs. (13) – (14), the following dimensionless expressions can be derived:

$$\frac{-\ln(|p|/p_0)}{\lambda z} = \left(\frac{\sqrt{1+I_c^2}+1}{2}\right)^{1/2} \tag{18a}$$

$$\frac{\Delta\theta}{\lambda z} = \left(\frac{\sqrt{1+I_c^2}-1}{2}\right)^{1/2} \tag{18b}$$

It can be noticed that, if $I_c \ll 1.0$, then $\lambda' \to \lambda$ (see Eq. (15')); thus Eq. (1) can be simplified as Eq. (11), which can also be deduced from Eq. (18a).

On the basis of Eqs. (18a) and (18b), the variations of "$-\ln(|p|/p_0)/\lambda z$" and "$\Delta\theta/\lambda z$" with "I_c" can be obtained, respectively, as shown in Fig. 13(a) and (b). For comparisons with the analytical predictions, the present experimental data (see Fig. 5) for the fine sand and the medium sand are also provided in these figures. Given the values of wave parameters and soil properties (see Table 2), the corresponding values of I_c in the present experiments can be calculated with Eq. (16). For the waves with $T = 1.2$ s, 1.5 s and 1.8 s, the corresponding values of I_c are 33.1, 50.4 and 67.1, respectively. Fig. 13(a) and (b) indicate that the analytical predictions of amplitude-attenuation and phase-lag generally match well with the experimental results. With the decrease of I_c, the values of "$-\ln(|p|/p_0)/\lambda z$" decrease remarkably, which approach 1.0 when $I_c < 1.0$; correspondingly, the values of $\Delta\theta/\lambda z$ also decrease, but approach zero when $I_c < 1.0$.

Under the condition of $I_c \gg 1.0$, Eqs. (18a)–(18b) can be further simplified as

$$\frac{-\ln(|p|/p_0)}{\lambda z} \approx \sqrt{\frac{I_c}{2}} \quad (\text{for } Ic \gg 1.0) \tag{19a}$$

$$\frac{\Delta\theta}{\lambda z} \approx \sqrt{\frac{I_c}{2}} \quad (\text{for } Ic \gg 1.0) \tag{19b}$$

As such, the phase-lag (temporal) and the amplitude-attenuation (spatial) can be closely correlated as follows:

$$\Delta\theta \approx -\ln(|p|/p_0) \quad (\text{for } Ic \gg 1.0) \tag{20}$$

By using such spatio-temporal correlation (Eq. (20)), the amplitude-attenuation of transient pore pressures can be directly predicted, only if the corresponding phase-lag is monitored in the offshore fields. As for the scenarios of natural wave conditions (e.g., the larger wave periods in the parametric study in Section 4.1), the values of I_c are usually of the order of 10^3 or more, which are larger than those ($10 < I_c < 10^2$) in the flume tests. As indicated by Fig. 13, both the amplitude-attenuation and the phase-lag along λz would be more remarkable for the larger values of I_c.

6. Conclusions

The spatio–temporal distributions of wave-induced pore pressures in a porous seabed are investigated physically and analytically. Based on the flume observations and analytical derivations, the following conclusions are drawn:

(1) Flume observations indicate that the amplitude-attenuation and the phase-lag phenomena are closely related to both wave parameters and soil properties. For a given soil depth, the pore pressure amplitude increases with increasing wave period; nevertheless, the phase-lag decreases with increasing wave period. The amplitude-attenuation and phase-lag along the non-dimensional soil depth are more significant for the fine sand than the medium sand.

(2) A relative rigidity of soil-skeleton to pore-fluid (R_k) is introduced to quantitatively evaluate the seabed compressibility. Explicit expressions for the amplitude-attenuation ($|p|/p_0$) and the phase-lag ($\Delta\theta$) are derived and further verified with the experimental results. Parametric analyses indicate that, as the relative rigidity (R_k) is much larger than 1.0, both the amplitude-attenuation and the phase-lag get more significant for larger wave period or for smaller values of the combined rigidity-permeability parameter of the soil.

(3) A non-dimensional parameter (I_c) is further derived to characterize the combined effects of wave parameters and soil properties on the spatio-temporal distributions of transient pore pressures under waves. A simplified spatio-temporal correlation of transient pore pressure is established, i.e., $\Delta\theta \approx -\ln(|p|/p_0)$ for $I_c \gg 1.0$, indicating the more rapidly the pore pressure amplitude attenuates within the seabed, the more significant the phase-lag becomes, correspondingly.

Declaration of competing interest

The authors declare that they have no known competing financial interests or personal relationships that could have appeared to influence the work reported in this paper.

Acknowledgements

This study was financially supported by the National Natural Science Foundation of China (Grant Nos. 11825205, 12061160463) and the Strategic Priority Research Program (Type-B) of Chinese Academy of Sciences (Grant No. XDB22030000). The technical assistances from Mr. Fu-lin Zhang in the flume experiments are greatly appreciated.

Appendix A. Compressibility and permeability of a porous seabed under wave loading

(1) Soil compressibility under 1D condition:

Under the natural conditions in the offshore fields, although the porous seabed is approximately full-saturated, a certain content of air can be entrapped in the pores of the soil. As such, the porous seabed is generally regarded as a three-phase medium, and its compressibility should be thereby attributed from soil-skeleton, pore-water, and the entrapped-air (see Fig. A1(a)). As aforementioned in Section 2.2, for the wave-seabed interactions, the soil layer with significant transient pore pressure responses is much shorter than the wave length, so that the pore pressure response under wave

loading can be essentially assumed as a quasi-one-dimensional (quasi-1D) process.

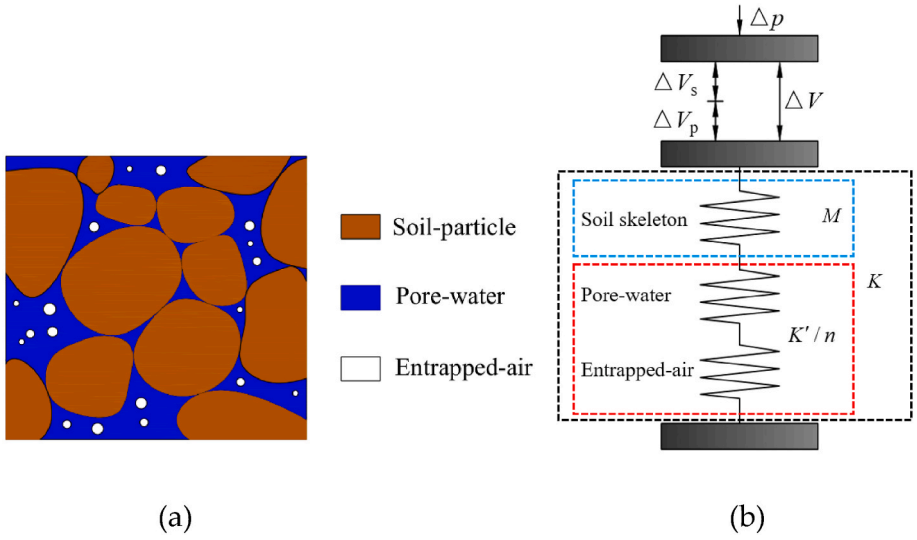

Fig. A1. Schematic diagram: (a) three-phase composition and (b) series spring analogy for the apparent bulk modulus of a porous seabed (Δp: external pressure exerting on the porous seabed; ΔV: volume compression of the porous seabed; ΔV_s: volume compression of the soil-skeleton; ΔV_p: volume compression of the pore-fluid; K: apparent bulk modulus of the porous seabed; M: apparent bulk modulus of the soil skeleton; $K^{'}$: apparent bulk modulus of the pore-fluid).

To characterize the soil compressibility under such quasi-1D condition, the series spring analogy method (see Cheng, 2016) is adopted for describing drained bulk modulus. As illustrated by Fig. A1(b), the change of total volume by compression of a porous seabed (ΔV) can be partitioned into a soil-skeleton part (ΔV_s) and a pore-fluid part (ΔV_p), i.e., $\Delta V = \Delta V_s + \Delta V_p$. For an ideal porous medium, i.e., a porous medium made of homogeneous and isotropic solid material, the apparent longitudinal rigidity (bulk modulus) of the porous medium (K) is related to that of soil-skeleton (M) and of pore-fluids ($K^{'}$):

$$\frac{1}{K}=\frac{1}{M}+\frac{n}{K^{'}} \tag{A1}$$

where n is the soil porosity.

In Eq. (A1), the longitudinal bulk modulus of soil-skeleton M (also known as the P-wave modulus, see Mavko et al., 2003) is defined as the ratio of axial stress to axial strain in a uniaxial strain state and can be expressed with shear modulus (G) and Poisson's ratio (ν) as

$$M=\frac{2(1-\nu)G}{1-2\nu} \tag{A2}$$

Correspondingly, the apparent bulk modulus of the pore-fluid $K^{'}$ can be calculated with:

$$K^{'}=\left(\frac{1}{K_w}+\frac{1-S_r}{P_0}\right)^{-1} \tag{A3}$$

where K_w is the true bulk modulus of pure water (e.g., $K_w \approx 2.2 \times 10^9$ Pa at 20 °C and 1 Atm), P_0 is the absolute pore water pressure and S_r is the degree of saturation (Verruijt, 1969). Eq. (A3) indicates that the compressibility of the pore-fluid is sensitive to the gas content or the degree of saturation, as the entrapped-air is much more compressible than the pure water.

(2) Soil permeability:

The continuous void spaces in a porous medium allow the pore-water to seep through. Permeability is defined as the property of a soil that allows the seepage of fluids through its interconnected void spaces. Previous studies have indicated that soil permeability is a function of both the void ratio (e) and degree of saturation (S_r). A widespread relationship between the permeability and properties of pores was proposed by Kozeny (1927) and later modified by Carman (1937, 1938, 1956), which is well-known as the Kozeny-Carman (KC) equation (Carman, 1956). This equation has taken several semi-empirical and semi-theoretical forms, including the following one (see Chapuis and Aubertin, 2003):

$$\log(k_{sat})=A+\log\left[\frac{e^3}{S^2G_s^2(1+e)}\right] \tag{A4}$$

where k_{sat} is the coefficient of permeability for a saturated soil, the factor A characterizes the shape and tortuosity of channels, S is the specific surface (m^2/kg of soil grains), G_s is the specific weight of soil. It yielded the saturated permeability as a function of the void ratio, the specific surface and a factor taking into account the shape and tortuosity of channels. Carman (1939) suggested that the value of A should be within the range of 0.29–0.51. The value of the specific surface S can be well evaluated with the grain size distribution according to the method by Chapuis and Légaré (1992). Mualem (1976) proposed a simplified equation to evaluate the permeability of an unsaturated soil, which is expressed as

$$\frac{k_s}{k_{sat}}=\frac{(S_r-S_0)^3}{(1-S_0)^3} \tag{A5}$$

where k_s is the permeability of the soil with degree of saturation S_r, k_{sat} is the permeability with full saturation, S_0 is the degree of saturation corresponding to a residual water content taken as 0.2 for sand and gravel (see Chapuis and Aubertin, 2003).

As a case study, the variations of permeability (k_s) for fine sands with void ratio (e) for various of saturation degrees (S_r) are given in Fig. A2. The specific surface S of the examined fine sands with grain size distribution in Fig. 3 is chosen as $S = 27.34$ m^2/kg, and A is chosen as $A = 0.5$. It is indicated that k_s increases overwhelmingly with increasing e. For a fixed value of e, k_s increases slightly with S_r for a nearly saturated sand (e.g., $S_r \approx 0.985$–1.0). As shown in Fig. A2, the measured permeability of the present fine sand ($k_s = 9.60 \times 10^{-5}$ m/s, for $e = 0.67$ and $S_r = 0.993$) matches well with the predicted results by Eq. (A4)-(A5).

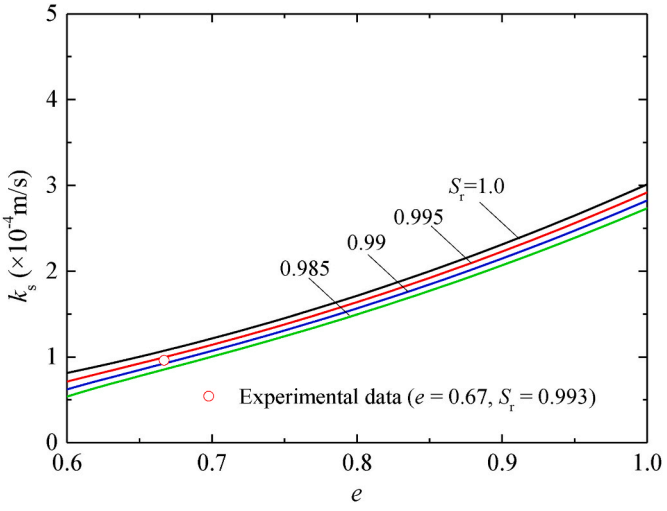

Fig. A2. k_s vs. e for various values of S_r ($G_s = 2.65$, $S = 27.34$ m^2/kg, $A = 0.5$).

References

Biot, M.A., 1941. General theory of three-dimensional consolidation. J. Appl. Phys. 12 (2), 155–164.

Carman, P.C., 1937. Fluid Flow through Granular Beds. Transactions, vol. 15. Institution of Chemical Engineers, London, pp. 150–166.

Carman, P.C., 1938. Determination of the specific surface of powders I. Trans. J. Soc. Chem. Ind. 57, 225–234.

Carman, P.C., 1939. Permeability of saturated sands, soils and clays. J. Agric. Sci. 29, 263–273.

Carman, P.C., 1956. Flow of Gases through Porous Media. Butterworths, London.

Chapuis, R.P., Aubertin, M., 2003. On the use of the Kozeny-Carman equation to predict the hydraulic conductivity of soils. Can. Geotech. J. 40 (3), 616–628.

Chapuis, R.P., Légaré, P.P., 1992. A simple method for determining the surface area of fine aggregates and fillers in bituminous mixtures. In: Effects of Aggregates and Mineral Fillers on Asphalt Mixture Performance, vol. 1147. American Society for Testing and Materials, ASTM STP, pp. 177–186.

Cheng, A.H.-D., 2016. Poroelasticity. Springer Nature, Switzerland.

Christian, J.T., Taylor, P.K., Yen, J.K.C., 1974. Large diameter underwater pipeline for nuclear power plant designed against soil liquefaction. In: *Proceedings of the 6th Annual Offshore Technology Conference*, pp. 597–606. Huston.

Gao, F.P., 2003. FEM simulation of response of non-homogeneous sandy seabed of finite thickness to non-linear ocean wave loading. Shipbuild. China 44 (Suppl. l), 447–452.

de Groot, M.B., Kudella, M., Meijers, P., Oumeraci, H., 2006. Liquefaction phenomena underneath marine gravity structures subjected to wave loading. J. Waterw. Port, Coast. Ocean Eng. 132, 325–335.

Hsu, J.R.C., Jeng, D.S., 1994. Wave-induced soil response in an unsaturated anisotropic seabed of finite thickness. Int. J. Numer. Anal. Methods GeoMech. 18 (11), 785–807.

Jeng, D.S., Hsu, J.R.C., 1996. Wave-induced soil response in a saturated seabed of finite thickness. Geotechnique 46 (3), 427–440.

Jeng, D.S., Seymour, B., Gao, F.P., Wu, Y.X., 2007. Ocean waves propagating over a porous seabed: residual and oscillatory mechanisms. Sci. China Technol. Sci. 50 (1), 81–89.

Jeng, D.S., 2018. Mechanics of Wave-Seabed-Structure Interactions: Modelling, Processes and Applications. Cambridge University Press, Cambridge.

Knappett, J.A., Craig, R.R.F., 2012. Craig's Soil Mechanics. Taylor & Francis, London.

Kozeny, J., 1927. Ueber kapillare leitung des wassers im Boden. Sitzungsberichte Wiener Akademie 136 (2a), 271–306.

Li, X.J., Gao, F.P., Yang, B., Zang, J., 2011. Wave-induced pore pressure responses and soil liquefaction around pile foundation. Int. J. Offshore Polar Eng. 21 (3), 233–239.

Liu, B., Jeng, D.S., Ye, G.L., Yang, B., 2015. Laboratory study for pore pressures in sandy deposit under wave loading. Ocean. Eng. 106, 207–219.

Madsen, O.S., 1978. Wave-induced pore pressures and effective stresses in a porous bed. Geotechnique 28 (4), 377–393.

Maeno, Y., Hasegawa, T., 1985. Evaluation of wave-induced pore pressure in sand layer by wave steepness. Coast Eng. J. 28, 31–44.

Mavko, G., Mukerji, T., Dvorkin, J., 2003. The Rock Physics Handbook. Cambridge University Press, 2003.

Michallet, H., Mory, M., Piedra-Cueva, I., 2009. Wave-induced pore pressure measurements near a coastal structure. J. Geophys. Res. 114 (C6). C06019.

Miyamoto, T., Yoshinaga, S., Soga, F., 1989. Seismic prospecting method applied to the detection of offshore breakwater units setting in the bed. Coast Eng. J. 32, 103–112.

Mory, M., Michallet, H., Bonjean, D., et al., 2007. A field study of instantaneous liquefaction caused by waves around a coastal structure. J. Waterw. Port, Coast. Ocean Eng. 133 (1), 28–38.

Moshagen, H., Tørum, A., 1975. Wave induced pressures in permeable seabeds. J. Waterw., Harbors Coastal Eng. Div., Am. Soc. Civ. Eng. 101 (1), 49–57.

Mualem, Y., 1976. A new model for predicting the hydraulic conductivity of unsaturated porous media. Water Resour. Res. 12, 513–522.

Okusa, S., 1985. Wave-induced stresses in unsaturated submarine sediments. Geotechnique 35 (4), 517–532.

Putnam, J.A., 1949. Loss of wave energy due to percolation in a permeable sea bottom. Trans. Am. Geophys. Union 30 (3), 349–356.

Qi, W.G., Gao, F.P., 2014a. Physical modeling of local scour development around a large-diameter monopile in combined waves and current. Coast. Eng. 83, 72–81.

Qi, W.G., Gao, F.P., 2014b. Equilibrium scour depth at offshore monopile foundation in combined waves and current. Sci. China Technol. Sci. 57 (5), 1030–1039.

Qi, W.G., Gao, F.P., 2018. Wave induced instantaneously-liquefied soil depth in a non-cohesive seabed. Ocean. Eng. 153, 412–423.

Qi, W.G., Li, C.F., Jeng, D.S., Gao, F.P., Liang, Z.D., 2019. Combined wave-current induced excess pore-pressure in a sandy seabed: flume observations and comparisons with theoretical models. Coast. Eng. 147 (MAY), 89–98.

Qi, W.G., Shi, Y.M., Gao, F.P., 2020. Uplift soil resistance to a shallowly-buried pipeline in the sandy seabed under waves: poro-elastoplastic modeling. Appl. Ocean Res. 95, 102024.

Reid, R.O., Kajirua, K., 1957. On the damping of gravity waves over a permeable seabed. Trans. Am. Geophys. Union 38 (5), 662–666.

Sarpkaya, T., 2010. Wave Forces on Offshore Structures. Cambridge University Press, Cambridge.

Smith, A.W.S., Gordon, A.D., 1983. Large breakwater toe failures. J. Waterw. Port, Coast. Ocean Eng. 109 (2), 253–255.
Sumer, B.M., Fredsøe, J., 2002. The Mechanism of Scour in the Marine Environment. World Scientific, New Jersey.
Sumer, B.M., Fredsøe, J., Christensen, S., Lind, M.T., 1999. Sinking/floatation of pipelines and other objects in liquefied soil under waves. Coast. Eng. 38, 53–90.
Sumer, B.M., 2014. Liquefaction Around Marine Structures. World Scientific Publishing Co., Singapore.
Verruijt, A., 1969. Elastic storage of aquifers. In: Flow through Porous Media. Academic Press, New York, pp. 331–376.
Yamamoto, T., Koning, H.L., Sellmeijer, H., Hijum, E.V., 1978. On the response of a poro-elastic bed to water waves. J. Fluid Mech. 87 (1), 193–206.
Zen, K., Yamazaki, H., 1990. Mechanism of wave-induced liquefaction and densification in seabed. Soils Found. 30 (4), 90–104.